NASA TN D-1049

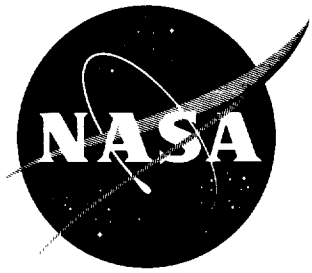

TECHNICAL NOTE

D-1049

ANNULAR INTERNAL-EXTERNAL-EXPANSION ROCKET NOZZLES

FOR LARGE BOOSTER APPLICATIONS

By James F. Connors, Robert W. Cubbison, and
Glenn A. Mitchell

Lewis Research Center
Cleveland, Ohio

NATIONAL AERONAUTICS AND SPACE ADMINISTRATION

WASHINGTON September 1961

NATIONAL AERONAUTICS AND SPACE ADMINISTRATION

TECHNICAL NOTE D-1049

ANNULAR INTERNAL-EXTERNAL-EXPANSION ROCKET NOZZLES FOR LARGE BOOSTER APPLICATIONS

By James F. Connors, Robert W. Cubbison, and
Glenn A. Mitchell

SUMMARY

For large-thrust booster applications, annular rocket nozzles employing both internal and external expansion are investigated. In these nozzles, free-stream air flows through the center as well as around the outside of the exiting jet. Flaps for deflecting the rocket exhaust are incorporated on the external-expansion surface for thrust-vector control.

In order to define nozzle off-design performance, thrust vectoring effectiveness, and external stream effects, an experimental investigation was conducted on two annular nozzles with area ratios of 15 and 25 at Mach 0, 2, and 3 in the Lewis 10- by 10-foot wind tunnel. Air, pressurized to 600 pounds per square inch absolute, was used to simulate the exhaust flow. For a nozzle-pressure-ratio range of 40 to 1000, the ratio of actual to ideal thrust was essentially constant at 0.98 for both nozzles. Compared with conventional convergent-divergent configurations on hypothetical boost missions, the performance gains of the annular nozzle could yield significant orbital payload increases (possibly 8 to 17 percent). A single flap on the external-expansion surface of the area-ratio-25 annular nozzle produced a side force equal to 4 percent of the axial force with no measurable loss in axial thrust.

INTRODUCTION

Currently, for rocket booster application convergent-divergent (herein called C-D) nozzles are being considered in either single or clustered motor arrangements. In order to avoid large overexpansion penalties (or thrust losses) at takeoff pressure ratios, relatively low area ratios must be used with C-D nozzles. High-area-ratio nozzles, however, are attractive for improved performance at altitude. With cold air at a chamber pressure of 600 pounds per square inch absolute an area-ratio-25 C-D nozzle would attain only about 80 percent of ideal thrust at sea level, whereas an area-ratio-8 C-D nozzle under these conditions will produce approximately 95 percent of ideal thrust.

External-expansion nozzles, on the other hand, offer good "off-design" performance because overexpansion is avoided by means of a free-expansion boundary. The ratio of actual to ideal thrust remains high and insensitive to nozzle pressure ratio at less than design value, and thus high area ratios can be used to improve altitude performance without compromising takeoff capability.

In the present study an unconventional annular-nozzle configuration utilizing a combination of internal and external expansion of the rocket exhaust is investigated. Free-stream air flows through the center as well as around the outside of the exiting jet and, in effect, alleviates any base heating problems. Flaps are installed on the external-expansion surface to deflect the jet for thrust-vector control. In concept, the annular nozzle would be fed by a single combustor or by a multitude of burners, as advocated for the plug nozzle (ref. 1). Thus, the annular nozzle could be considered as a refined cluster configuration.

To investigate the aerodynamic characteristics of these internal-external-expansion annular rocket nozzles, an experimental study was conducted in the Lewis 10- by 10-foot supersonic wind tunnel. Two annular nozzles with area ratios of 15 and 25 were evaluated in quiescent air and at Mach 2 and 3. Jet simulation over a pressure-ratio range of 40 to 1000 was accomplished with cold air pressurized to 600 pounds per square inch absolute. For these conditions, nozzle thrust performance, thrust-vectoring effectiveness of two jet-deflection flaps, and external stream effects were determined.

SYMBOLS

A_e projected nozzle-exit area

A_{th} nozzle throat area

C_F thrust coefficient, F_n/P_cA_{th}

F_n net thrust

$F_{n,id}$ ideal net thrust, mV_{id}

l axial distance from throat to trailing edge of external ramp

M Mach number

m nozzle mass-flow rate

N_F normal force

P total pressure

p static pressure

V_{id} ideal nozzle-exit velocity

x axial distance from throat

ϵ nozzle area ratio, A_e/A_{th}

θ flap deflection angle

Subscripts:

c combustion chamber

N nozzle

R rake

0 free stream

ANNULAR-NOZZLE DESIGN CONSIDERATIONS

The evolution of the annular-nozzle concept from equivalent C-D nozzle systems is illustrated in figure 1. To achieve a given large thrust level, three different approaches may be considered. First, a conventional motor might be used. A single large nozzle (fig. 1(a)) would be long and would have base heating and gimbaling problems. Second, a number of rocket motors might be employed. A cluster of smaller but geometrically similar nozzles (fig. 1(b)) would, of course, be much shorter and would probably allow more refined vector control by gimbaling only the outer motors. However, difficult jet interactions and base heating problems would arise with attendant weight penalties (e.g., heat shields). As a third approach, an annular design (fig. 1(c)) would eliminate the base heating problems by allowing external free-stream air to flow through the center. This nozzle would also be short and could be considered the result of integrating a cluster of individual nozzles into one annular configuration.

Some cursory consideration of the nozzle cooling requirements is shown in figure 2. Comparisons are made between single and annular C-D nozzles of equal throat areas, divergence angles, and area ratios. Herein the assumption is made that the heat-flux distribution through the nozzle is a function only of the one-dimensional area variation; thus

cooling requirements would be reflected in the relative amounts of local surface area. With increasing radius ratio (larger annular ring diameters) length decreases rapidly, while both the supersonic (divergent) and sonic throat wetted areas remain constant and equal for both the single conventional and annular C-D nozzles. In this case the length of the throat region is conservatively assumed to be one hydraulic diameter; throat wetted area is then equal to the product of the total wetted perimeter and the hydraulic diameter. From this simple geometric scaling consideration it might be concluded that the total heat load would be about the same for the annular as for the single conventional C-D nozzle. This annular arrangement with external expansion might appear even more favorable from a cooling standpoint, since a portion of the jet would be contained by a free-expansion boundary with no cooling requirement.

From aerodynamic considerations, a combination of both internal and external expansion was selected, the external expansion to improve the nozzle off-design performance characteristics and the internal expansion to minimize boattail angle and the inclination of the sonic line. For design conditions Prandtl-Meyer flow relations were used to describe both the internal- and external-expansion processes. Internal flow expansion occurred about a point on the theoretical throat line, and external expansion in the opposite direction took place about the nozzle lip. The flow patterns at less than, equal to, and greater than design pressure ratio are illustrated in figure 3. By virtue of a free-expansion boundary which adjusts according to the pressure ratio, the flow remains attached to and follows the external surface at all conditions. Therefore, at less than design pressure ratio, overexpansion penalties would not be incurred, because the pressures on the external ramp would not fall below ambient. The internal expansion was limited to area ratios corresponding to the full nozzle pressure ratio at sea level (or launch) conditions. At design altitude the flow exits from the nozzle in a uniform stream paralleling the axis. Above design the flow would continue to expand beyond the nozzle without affecting the ramp pressures. The exiting jet would then be mainly flaring out from or into the nozzle centerline, depending on the orientation of the expansion surfaces.

APPARATUS AND PROCEDURE

An experimental study of two such annular internal-external-expansion nozzle configurations was conducted in the 10- by 10-foot supersonic wind tunnel at Mach numbers of 0, 2, and 3 and simulated pressure altitudes up to 75,000 feet. The specific aerodynamic design details are shown in figure 4. Nozzles with expansion ratios ϵ of 15 and 25 were designed with equal throat areas (3.02 sq in.). Theoretically, the flow was expanded internally through an isentropic Prandtl-Meyer turning process to Mach numbers of 3.145 and 3.29 for the ϵ = 15 and 25 nozzles, respectively. This corresponds to essentially complete expansion for simulated launch conditions at a chamber pressure of 600 pounds per square inch absolute ($P_c/p_0 \approx 40$).

For the initial throat radii selected, the Prandtl-Meyer turning center was located on the inner radius for $\epsilon = 15$ and on the outer radius for $\epsilon = 25$. For the purposes of this study (i.e., nozzle performance evaluation) contoured isentropic external-expansion ramps were used. However, some experimental data exist in the literature to support the supposition that thrust performance would be little affected by shortening the ramp through the use of a straight conical surface. This latter modification was not examined in the present study.

Hardware details of the annular nozzles, the test model, and the tunnel installation are shown in the cutaway drawings of figure 5 and the photographs of figure 6. The nozzle outer diameters are approximately 9 and 15 inches for $\epsilon = 15$ and 25, respectively. Provisions were made in the external-expansion surface to install attitude control flaps in the pitch plane. Flaps with deflection angles of 0°, 10°, and 20° could be installed either singly or in pairs as shown in figure 6(c). In either case the flaps extended from the trailing edge forward 4.9 inches and were 1.748 inches wide. When both flaps were installed, 7.26 percent of the exit circumference was deflected on the $\epsilon = 25$ nozzle and 27.8 percent on the $\epsilon = 15$ nozzle. By the addition of properly contoured wood blocks the width of the 20° top flap on the $\epsilon = 25$ nozzle was varied from 1.748 to 5.244 inches, that is, from 3.63 to 10.8 percent of the exit circumference.

In the present annular design concept the base region has been, in effect, relieved through the use of a bleed passage. Free-stream air is diverted (as shown by the dashed arrows in fig. 5), ducted back through the center of the annulus, and discharged parallel to the nozzle axis. The principal design consideration of the bleed passage was to employ gradual flow turning to prevent large losses and to have a passage of essentially constant area. Provisions were made on the $\epsilon = 15$ nozzle to reduce the bleed inlet area to give inlet- to exit-area ratios of approximately 1, 2, and 4.

High-pressure air was ducted through the main support strut into the model air line. A flexible bellows seal (shown in the upper sketch in fig. 5) was used to connect the model air line and nozzle air system in order to make nozzle force measurements possible. The high-pressure air (indicated by the solid arrows in fig. 5) was supplied to the nozzle by four support struts that discharged into an annular settling chamber ahead of the throat. These ducting requirements made the nozzle shrouds inordinately long in terms of an actual missile installation, but should not have affected the aerodynamic performance.

A conventional 15° half-angle convergent-divergent $\epsilon = 8$ nozzle having the same throat area as the annular nozzles was included in the investigation to establish the accuracy of the nozzle balance system through comparison of its performance with other existing data. The specific design details of this nozzle are not shown.

The axial force of the nozzle was measured by a pair of ring strain-gage links shown in figure 5. The balance links were mounted diametrically opposite each other with one end attached to the nozzle air system (active side of the balance) and the other end connected to the model air line (grounded side of the balance). Also shown in this view are the front and rear lift links used to measure the normal forces produced by the deflected flaps. The model skins surrounding the high-pressure air system were supported by a separate three-component balance system installed in the vicinity of the main support strut.

Eight total-pressure tubes were located in the small constant-area section downstream of the settling chamber and upstream of the convergent region ahead of the throat to measure the nozzle chamber pressure and to determine any peripheral distortion. Static-pressure taps were installed on the external nozzle surface to determine the flow expansion characteristics. Balance tare-force measurements were made from pitot-pressure rakes inside the nozzle air line in the bellows region, externally at the bleed-passage inlet, and at the nozzle exit. Static-pressure taps were located both inside and outside the bellows.

The primary parameters employed herein are nozzle thrust ratio and pressure ratio. Thrust ratio is defined as the ratio of net thrust (determined from jet-on and jet-off axial force measurements) to ideal thrust (calculated on the basis of complete isentropic expansion with uniform parallel flow at the exit). Nozzle pressure ratio is simply the ratio of chamber pressure to free-stream static pressure. In all cases there were no significant circumferential variations in chamber pressure at the nozzle approach and throat section. Nozzle weight flows were computed from the measured chamber pressure and the choked area at the throat. The $\epsilon = 8$ C-D nozzle was used as a calibration standard.

RESULTS AND DISCUSSION

Results were obtained in quiescent air and at Mach 2 and 3 over a nozzle-pressure-ratio range of 40 to 1000. For comparison purposes the performance levels of various convergent-divergent nozzles (ref. 2) are included with data obtained for the two annular configurations.

Nozzle Thrust Performance

Nozzle thrust characteristics are presented in figure 7. Performance is given as the ratio of net thrust to ideal thrust assuming isentropic expansion to ambient pressure. The thrust ratio of both annular nozzles (ϵ = 15 and 25) was essentially independent of pressure ratio at below-design conditions, remaining constant at approximately 98 percent. At simulated launch conditions ($P_c/p_0 \approx 40$) the area-ratio-25 annular

nozzle had a thrust ratio $F_n/F_{n,id}$ of 0.98, compared with 0.91 and 0.80 for a comparable $\epsilon = 25$ C-D nozzle with and without separation, respectively, and 0.95 for an $\epsilon = 8$ C-D nozzle. External expansion thus allows nozzles with higher area ratios to be used with at least the same "takeoff" thrust capability as for vehicles with conventional area-ratio-8 C-D nozzles. As evidenced by the data, there was no measurable effect of Mach number on the thrust performance of the annular nozzle (i.e., quiescent-air results were essentially the same as those obtained at Mach 2 and 3).

Performance data obtained with the $\epsilon = 8$ convergent-divergent nozzle are included in figure 7(c). Comparison of the data with those of reference 2 for an area-ratio-10 C-D nozzle shows generally good agreement.

Nozzle Flow Characteristics

Jet flow patterns for the $\epsilon = 15$ and 25 annular nozzles are shown in figure 8. Dotted lines have been added to the photographs to aid in identifying the external-expansion surfaces. The variation of flow expansion patterns with nozzle pressure ratio agrees quite well with the qualitative pictures of figure 3. At all nozzle pressure ratios the flow remained attached along the entire external-expansion surface. The free boundary of the jet adjusts with pressure ratio, being essentially parallel with the nozzle axis on design and expanding or contracting the jet flow above or below design, respectively.

Static-pressure distributions along the external-expansion surfaces are presented in figure 9 for the $\epsilon = 15$ and 25 annular nozzles, respectively. At and above design pressure ratios the experimental values agree very closely with the Prandtl-Meyer theoretical values. As indicated by the data, at the lower pressure ratios the flow alternately overexpanded and recompressed as it was turned back to the free-stream direction (as illustrated in fig. 3). No indication of nozzle flow separation is evident. Because of the limited data, the curves are not adequately defined and straight lines are used to connect the points. Based on the high thrust performance of these annular nozzles at less than design pressure ratio (fig. 7), it may be concluded that the associated turning losses on the external ramps were rather small.

Pitot-pressure profiles of the flow at the exit of the annular nozzles are shown in figure 10. The $\epsilon = 15$ nozzle was studied with both a constant-area and an expanding-area bleed passage through the center of the configuration. Regardless of the bleed area ratio, the discharge in the center of the jet was subsonic for all free-stream Mach numbers. With the $\epsilon = 25$ nozzle the center flow at the exit was supersonic at all supersonic Mach numbers. These exit profiles also show that the flow

did not separate from the external-expansion surface under any condition of pressure ratio or Mach number. With increasing pressure ratio, the annular height of the exiting jet increased as the external-expansion turning process continued.

Flap Thrust-Vectoring Effectiveness

A series of flow-deflection flaps installed on the external-expansion surfaces were investigated to determine their effectiveness in vectoring the thrust. The results are presented in figures 11 and 12 for the $\epsilon = 15$ and 25 annular nozzles, respectively. Because of the difficulty in measuring the small side-force components, there is a certain amount of scatter, and shaded bands are used to show the experimental trends. The ratio of normal force to the net thrust of the unvectored nozzle is given as a function of flap deflection angle. This ratio is essentially equal to the sine of the effective gimbal angle. For the $\epsilon = 15$ annular nozzle (fig. 11) with a single flap deflecting 13.9 percent of the circumference, a normal force of about 1.5 percent of net thrust was produced with a 20° deflection angle. When both flaps (top and bottom) were deflected, the resultant normal force was doubled. Figure 12 shows similar trends for the $\epsilon = 25$ nozzle. These data are for different Mach numbers and nozzle pressure ratios, but because of limited data, these individual effects could not be separated. When the width of the single flap on the $\epsilon = 25$ nozzle was increased from 3.63 to 10.9 percent of the circumference (fig. 13), the normal force increased about fourfold, the corresponding effective gimbal angle with one flap being of the order of 2°. Two flaps of this size (10.9 percent) should produce an effective gimbal angle of about 4.5°, according to the trends of the previous figures.

Thrust-vectoring efficiency is indicated in figure 14 as the ratio of net axial thrust with flaps deflected to that with undeflected flaps. Within the accuracy of thrust measurements there was no significant loss in thrust due to flap deflection on either the $\epsilon = 15$ or the $\epsilon = 25$ annular nozzles.

Overall Performance Comparison

In order to explore the significance of these improvements in nozzle thrust from an overall vehicle performance viewpoint, some cursory consideration was given to large booster applications. As shown in figure 15, a representative boost trajectory (altitude versus time) was assumed for a large (million-pound) vehicle. Corresponding thrust coefficients for three nozzle configurations (an $\epsilon = 25$ annular internal-external-expansion nozzle, an $\epsilon = 8$ and an $\epsilon = 25$ bell C-D nozzle) are also presented in this figure along with the thrust coefficient for a theoretical ideal nozzle. The superiority of the annular

nozzle over the $\epsilon = 8$ C-D nozzle occurs primarily at the higher altitudes and is indicated by the shaded area. Its superiority over the $\epsilon = 25$ bell C-D nozzle occurs at the lower altitudes and is indicated by the cross-hatched area. The time-integrated thrust coefficient for the $\epsilon = 25$ annular nozzle is 3 percent larger than that for the $\epsilon = 8$ C-D nozzle and 6 percent larger than that for the $\epsilon = 25$ bell C-D nozzle.

For comparison purposes, it was assumed that there is no significant difference in engine weights with the various nozzles. Because a cluster of C-D nozzles will probably require some heavy heat shields in the base area, this assumption of equal engine weights seems reasonable. For a multistage vehicle, the initial gross weight, the velocity increments of each stage, and the mass fractions of the upper stages were fixed. The results of the comparison indicate that the 3-percent improvement in thrust with the annular nozzle would allow up to 8 percent more orbital payload than the conventional C-D nozzle configuration. If a similar analysis is made on a large single-stage-to-orbit vehicle, the percentage improvement with the annular nozzle will be much larger (possibly by a factor of 2 or more). The exact amount of improvement is a very sensitive function of engine and vehicle parameters.

CONCLUDING REMARKS

An annular rocket nozzle having combined internal and external expansion with free-stream airflow through the center as well as around the outside of the exiting jet has been investigated. The annular configuration is, in essence, a refined cluster arrangement with excellent aerodynamic characteristics in terms of off-design performance, base flow phenomena, and thrust-vectoring capabilities.

Cold-flow experiments in quiescent air and at Mach 2 and 3 have demonstrated the performance characteristics of two such annular nozzles having area ratios of 15 and 25. At below-design conditions the ratio of thrust to ideal thrust was essentially independent of pressure ratio and constant at about 0.98 for both nozzles. No flow separation occurred within the nozzle over the entire pressure-ratio range studied (40 to 1000). A single flap deflecting the flow on the external-expansion surface of the area-ratio-25 annular nozzle (approximately 11 percent of the circumference) produced a side force equal to 4 percent of the axial force with no measurable loss in axial thrust.

With some crude assumptions regarding engine weights and for hypothetical boost missions, the performance for the area-ratio-25 annular nozzle indicated significant (possibly 8 to 17 percent) increases in orbital payload over vehicles using conventional convergent-divergent nozzles. Assessment of the overall merit of the annular configurations

more accurately necessitates detailed structural weight analyses. In practice, of course, for an actual installation the nozzle and upstream shroud lengths of the present geometries could be reduced considerably and other bleed inlet systems (e.g., flush slots) could be used without compromising the aerodynamic performance.

Lewis Research Center
National Aeronautics and Space Administration
Cleveland, Ohio, May 26, 1961

REFERENCES

1. Berman, K., and Crimp, F. W., Jr.: Performance of Plug-Type Rocket Exhaust Nozzles. ARS Jour., vol. 31, no. 1, Jan. 1961, pp. 18-23.

2. Farley, John M., and Campbell, Carl E.: Performance of Several Method-of-Characteristics Exhaust Nozzles. NASA TN D-293, 1960.

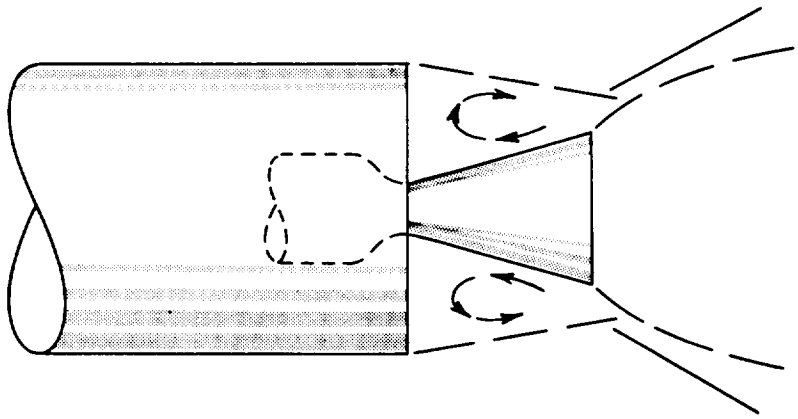

(a) Single large nozzle.

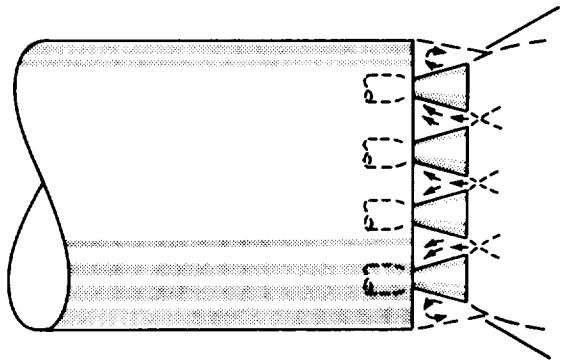

(b) Cluster of nozzles.

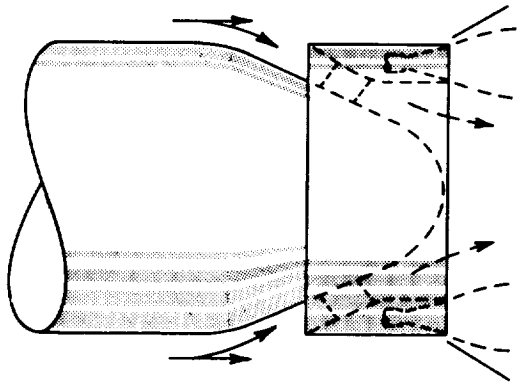

(c) Annular nozzle.

Figure 1. - Equivalent convergent-divergent nozzle systems for given large-thrust application.

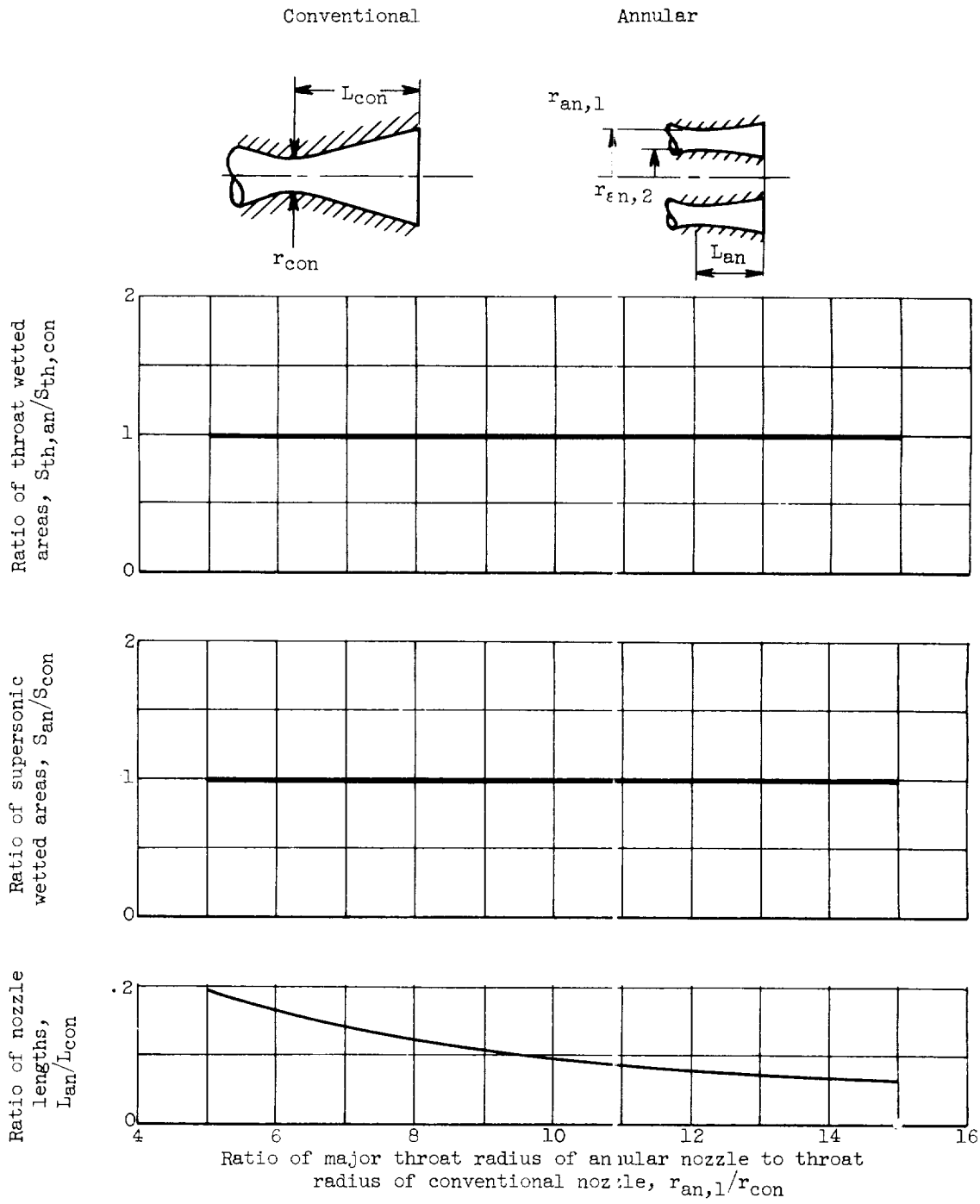

Figure 2. - Geometric comparison of annular and conventional nozzles.

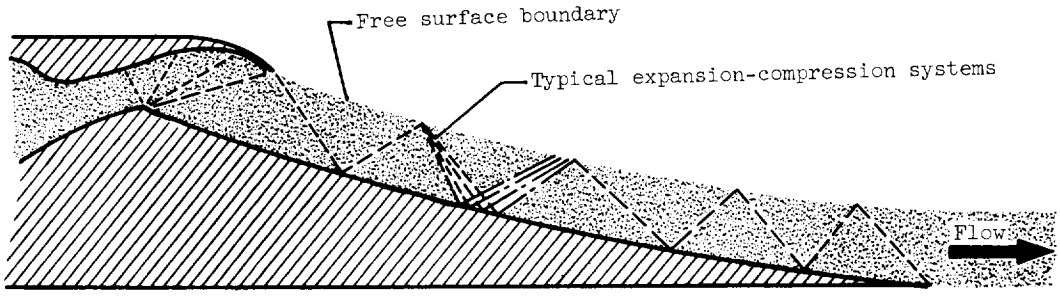

(a) Below-design pressure ratio.

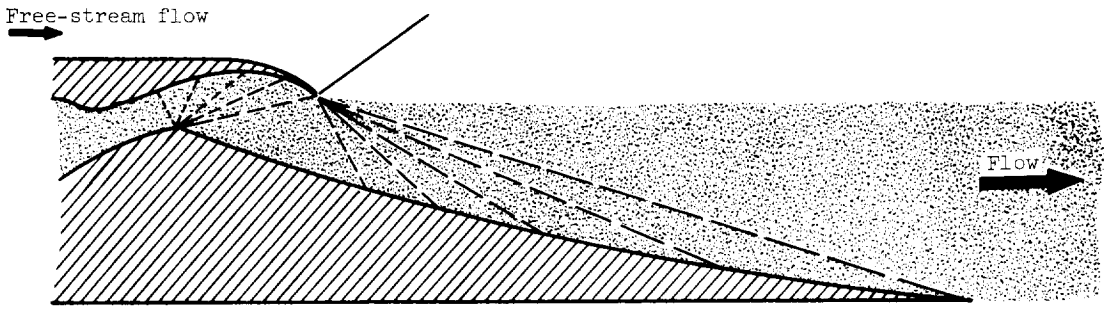

(b) Design pressure ratio.

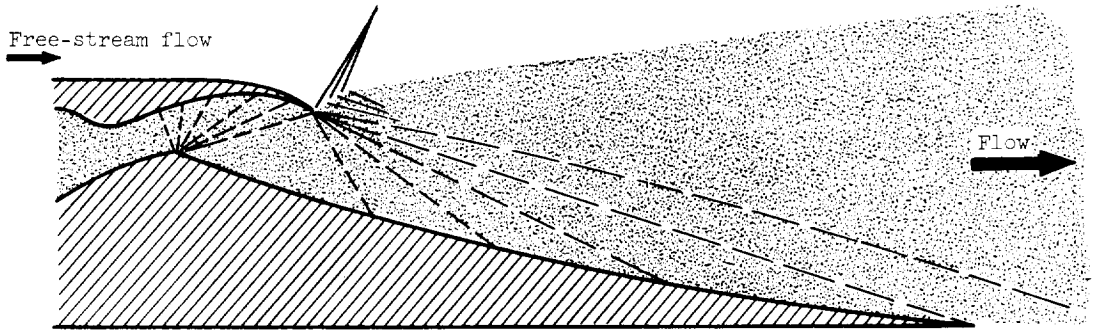

(c) Above-design pressure ratio.

Figure 3. - Exhaust flow patterns from isentropic internal-external-expansion nozzle.

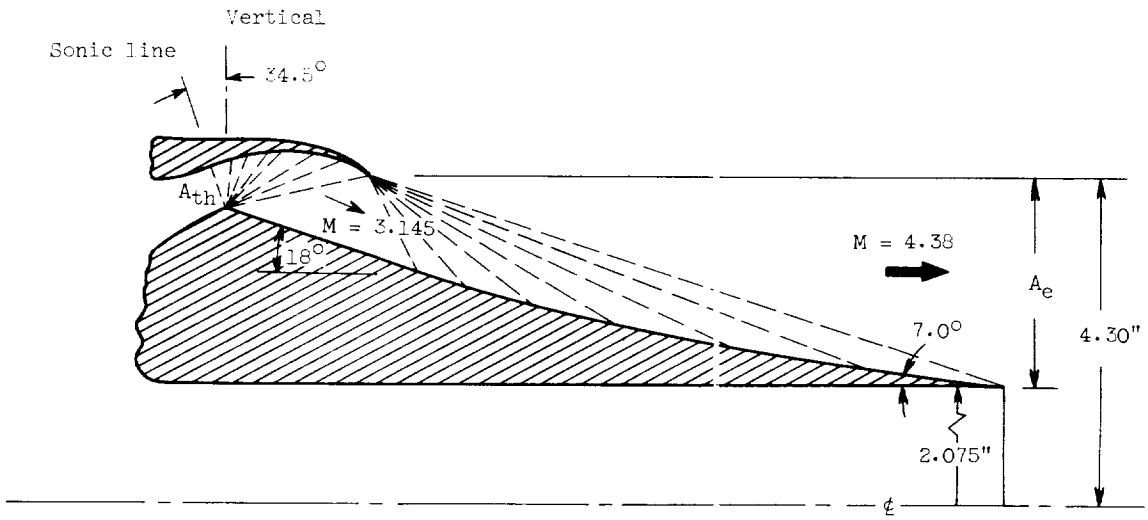

(a) Area ratio, ϵ, 15.

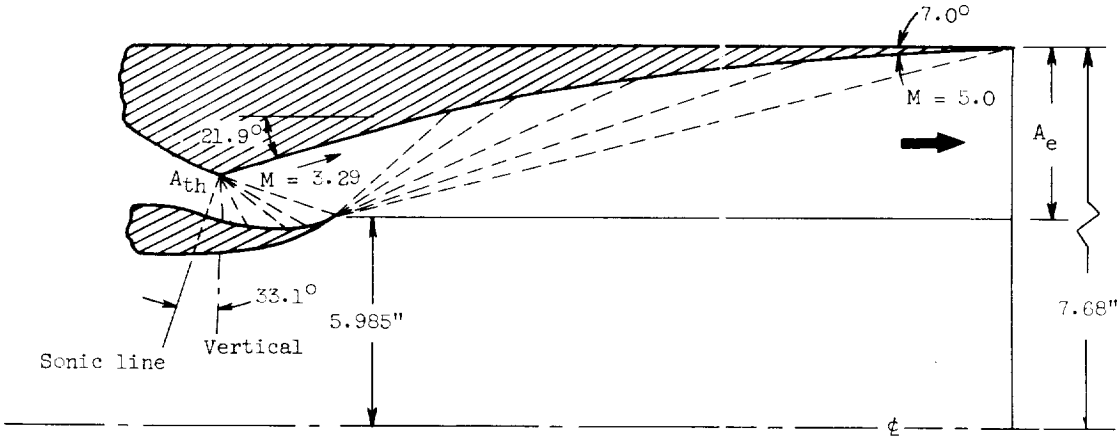

(b) Area ratio, ϵ, 25.

Figure 4. - Aerodynamic design details of annular nozzles.

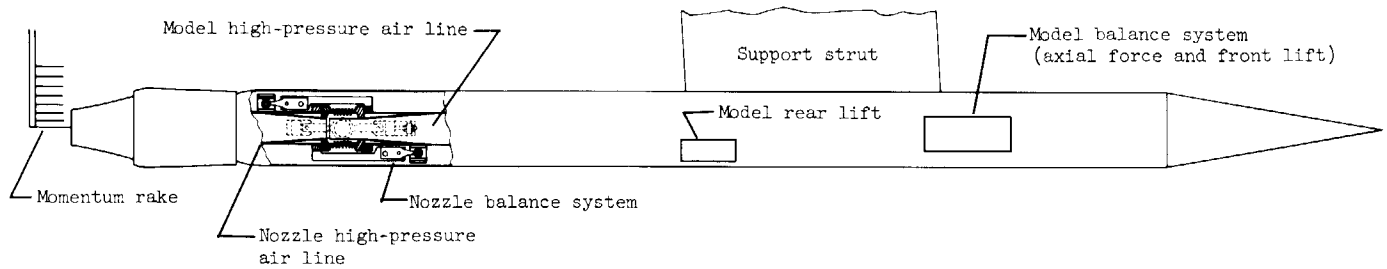

Overall view of model

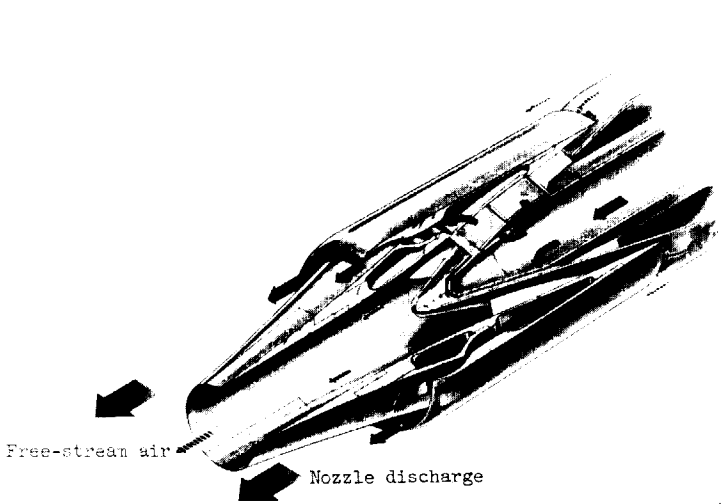

Area-ratio-15 nozzle

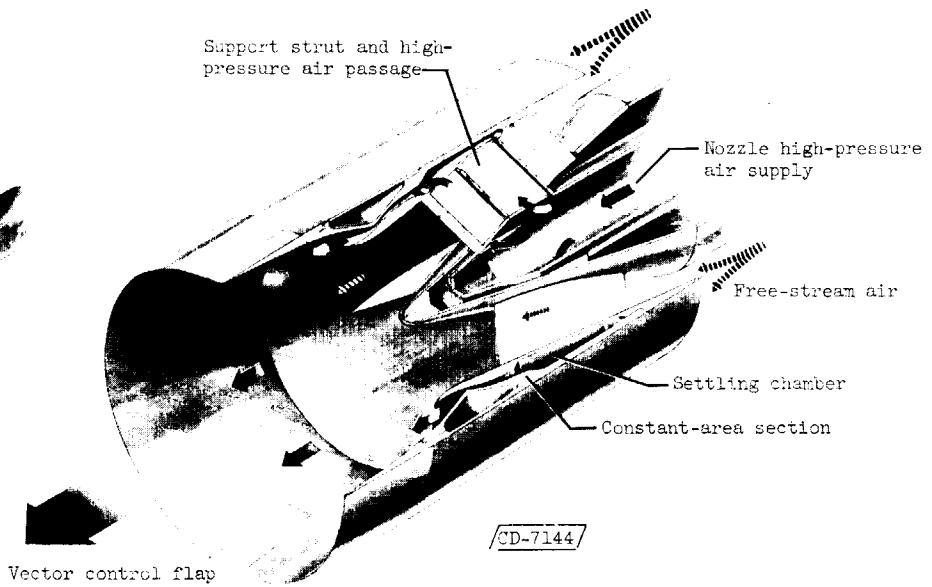

Area-ratio-25 nozzle

Figure 5. - Details of annular nozzles and model balance system.

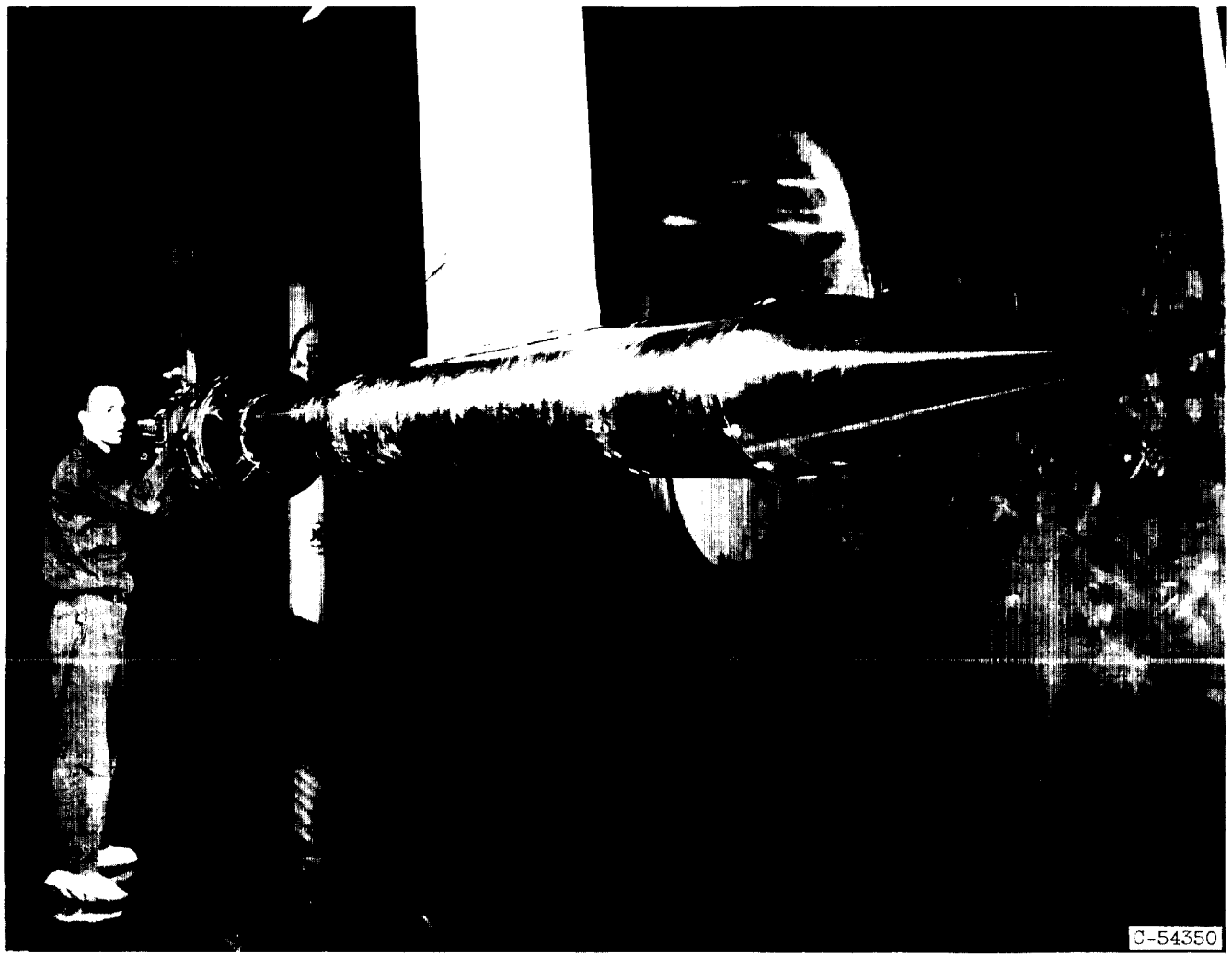

(a) Front view of area-ratio-25 nozzle.

Figure 6. - Photographs of model installed in 10- by 10-foot supersonic wind tunnel.

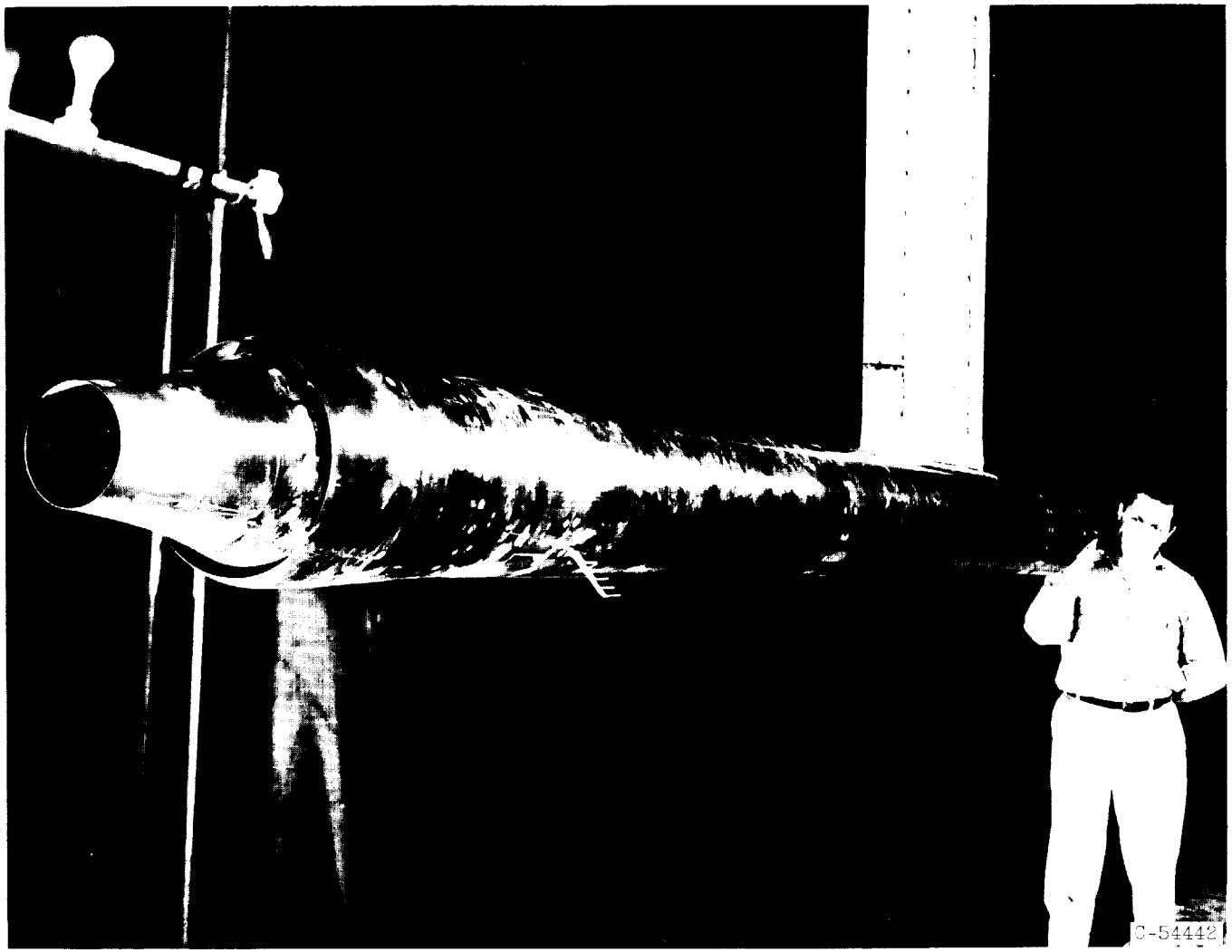

(b) Rear view of area-ratio-15 nozzle.

Figure 6. - Continued. Photographs of model installed in 10- by 10-foot supersonic wind tunnel.

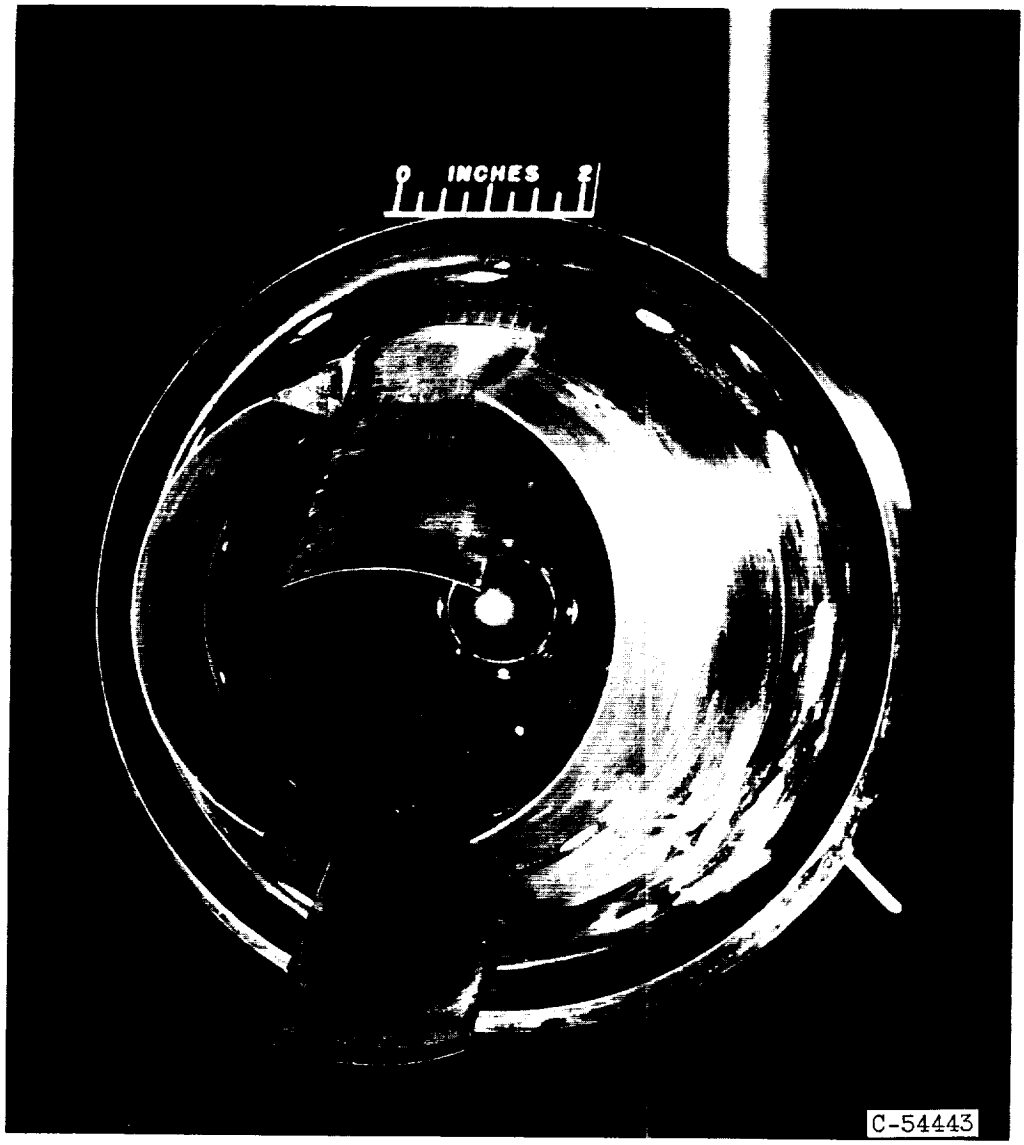

(c) Area-ratio-15 nozzle with flaps deflected.

Figure 6. - Continued. Photographs of model installed in 10- by 10-foot supersonic wind tunnel.

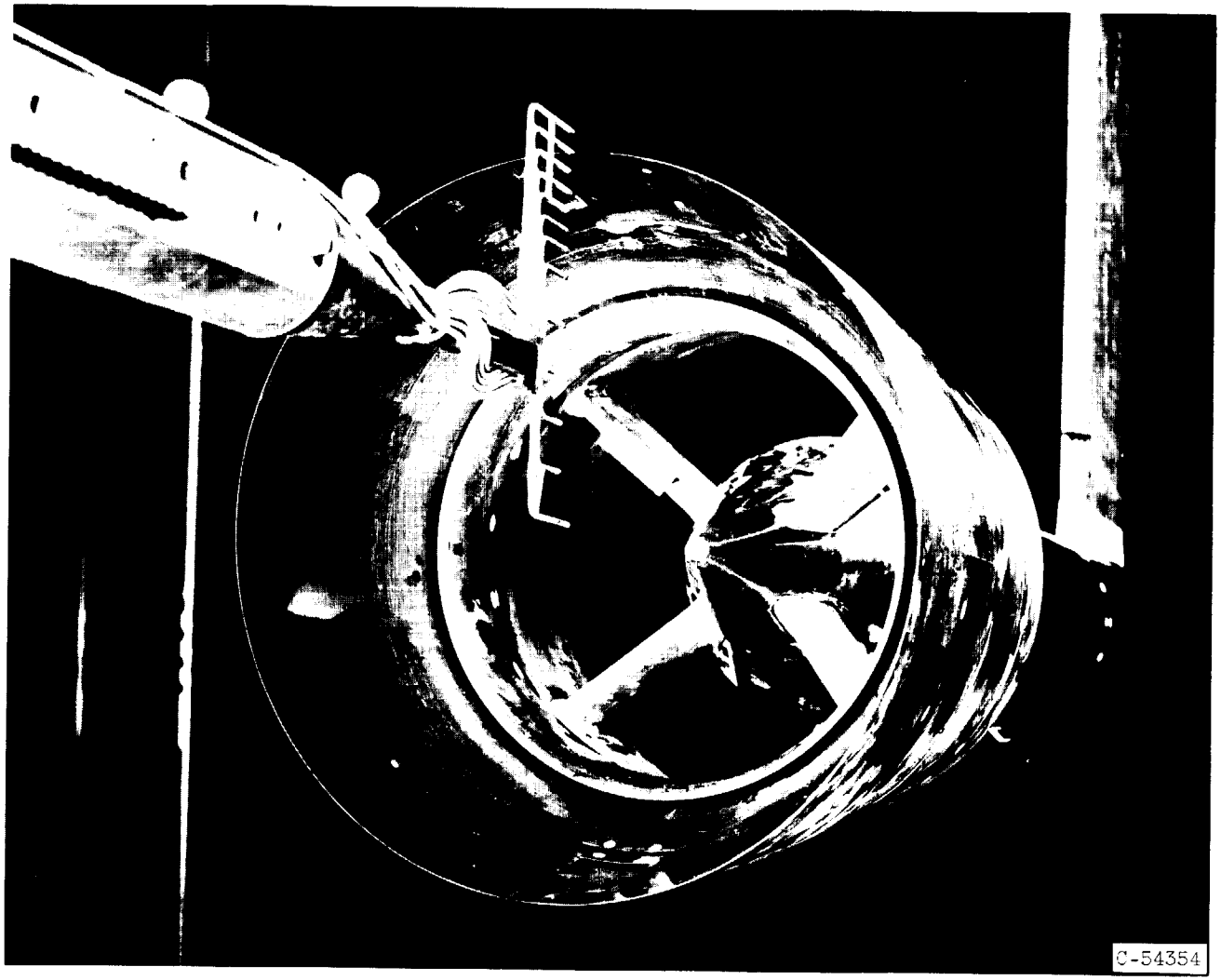

(d) Rear view of area-ratio-25 nozzle.

Figure 6. - Concluded. Photographs of model installed in 10- by 10-foot supersonic wind tunnel.

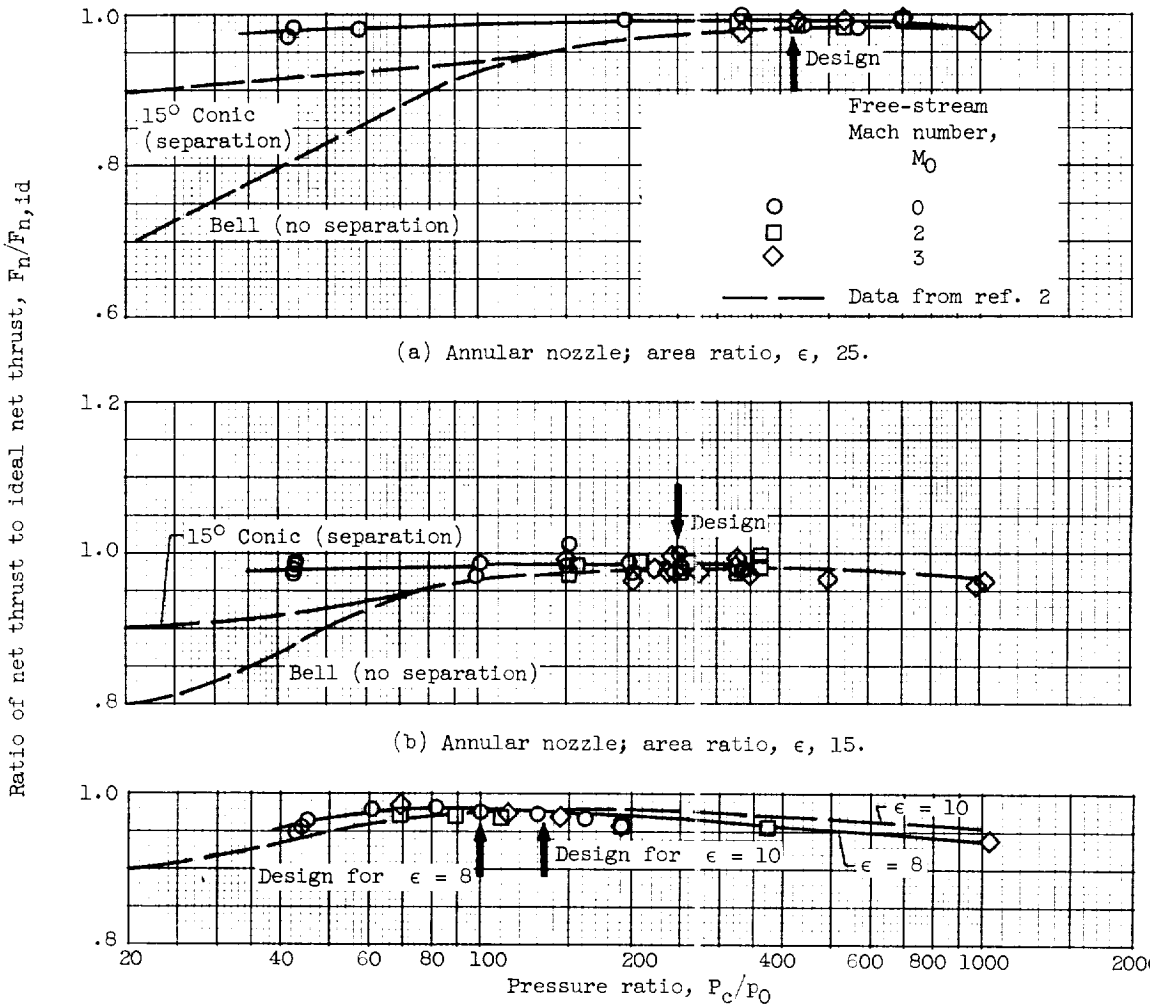

(a) Annular nozzle; area ratio, ϵ, 25.

(b) Annular nozzle; area ratio, ϵ, 15.

(c) 15° Conical convergent-divergent nozzle.

Figure 7. - Nozzle thrust performance.

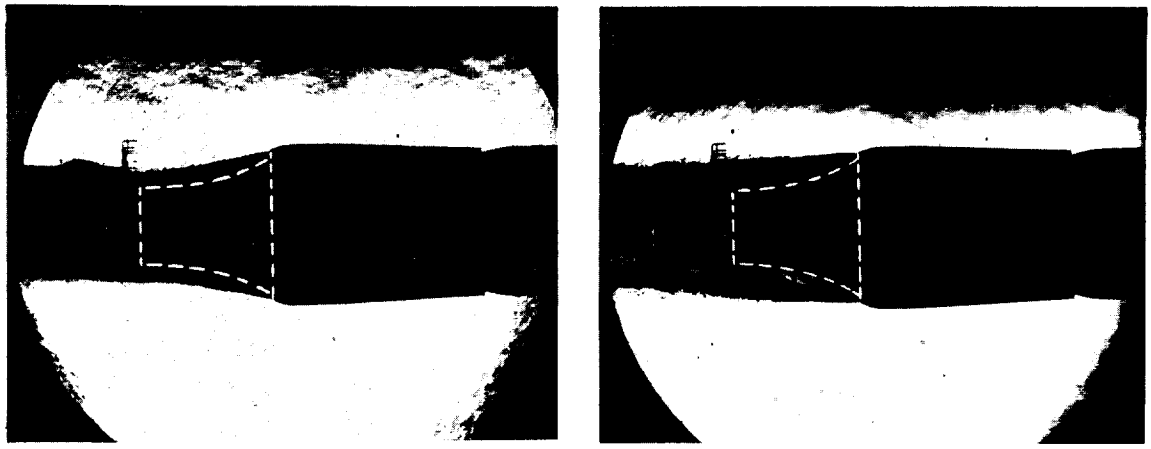

Pressure ratio, P_c/p_o = 43 P_c/p_o = 101

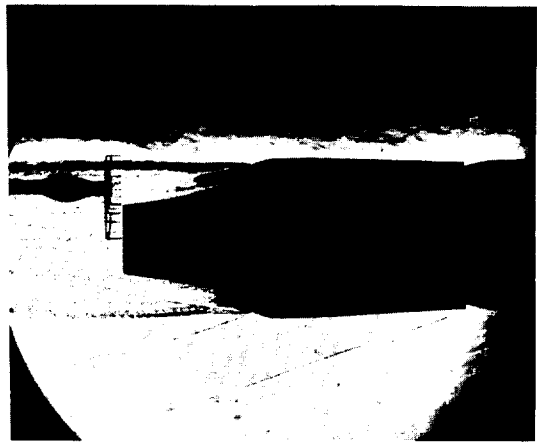

P_c/p_o = 222

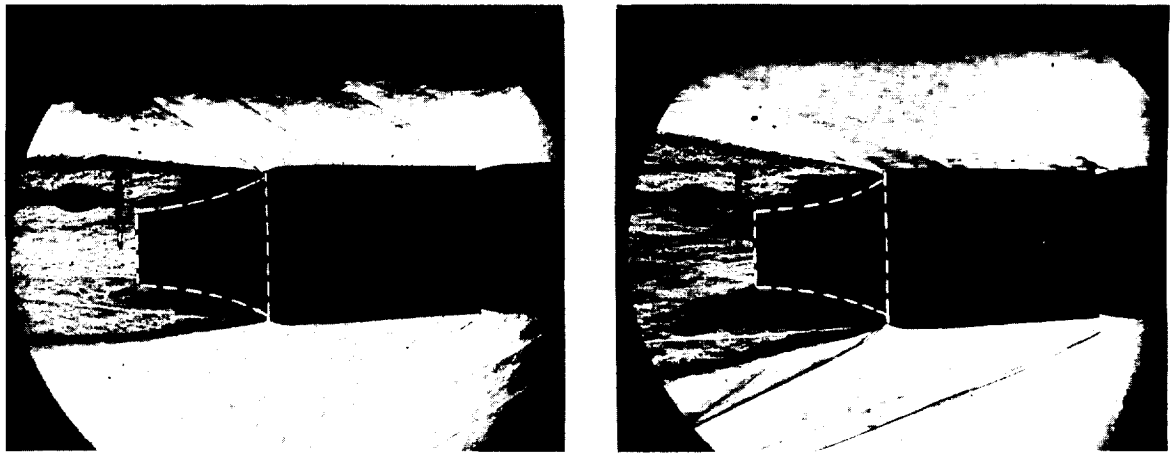

P_c/p_o = 367 C-56535 P_c/p_o = 1027

(a) Area ratio, ϵ, 15.

Figure 8. - Exit flow patterns for annular nozzles.

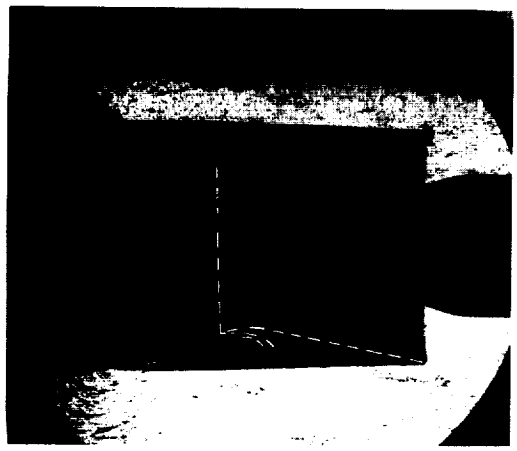

Pressure ratio, P_c/p_o = 42

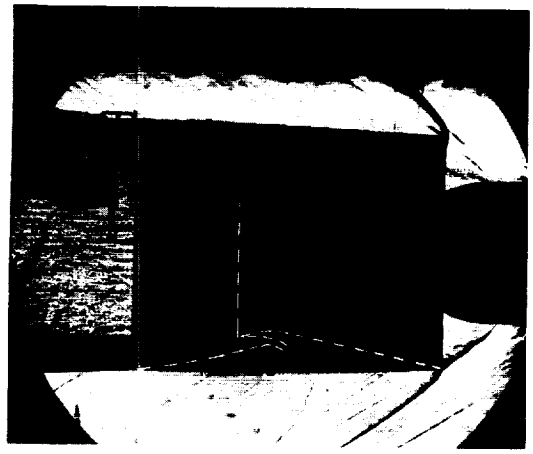

P_c/p_o = 329

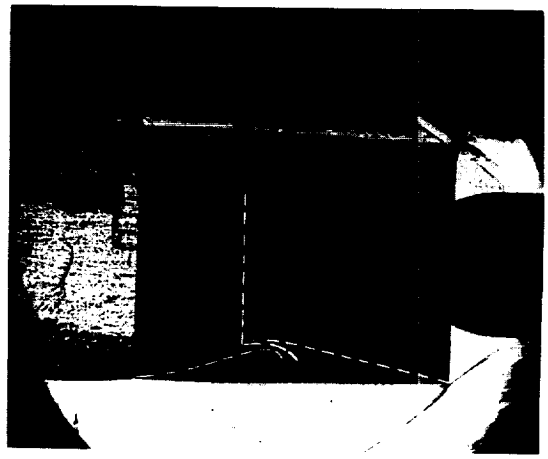

P_c/p_o = 538

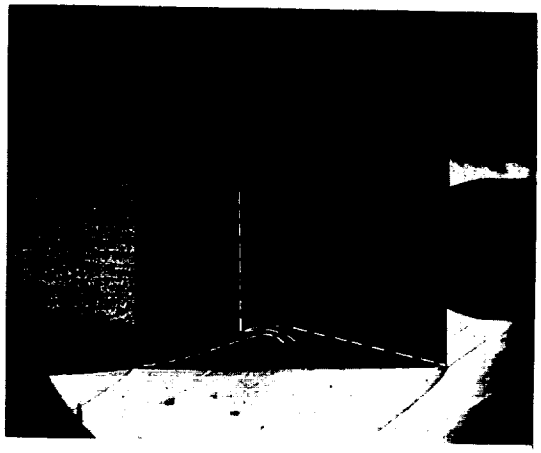

P_c/p_o = 695

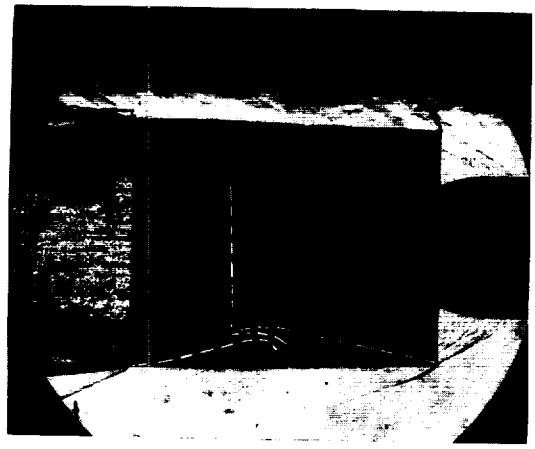

P_c/p_o = 1009

C-56534

(b) Area ratio, ϵ, 25.

Figure 8. - Concluded. Exit flow patterns for annular nozzles.

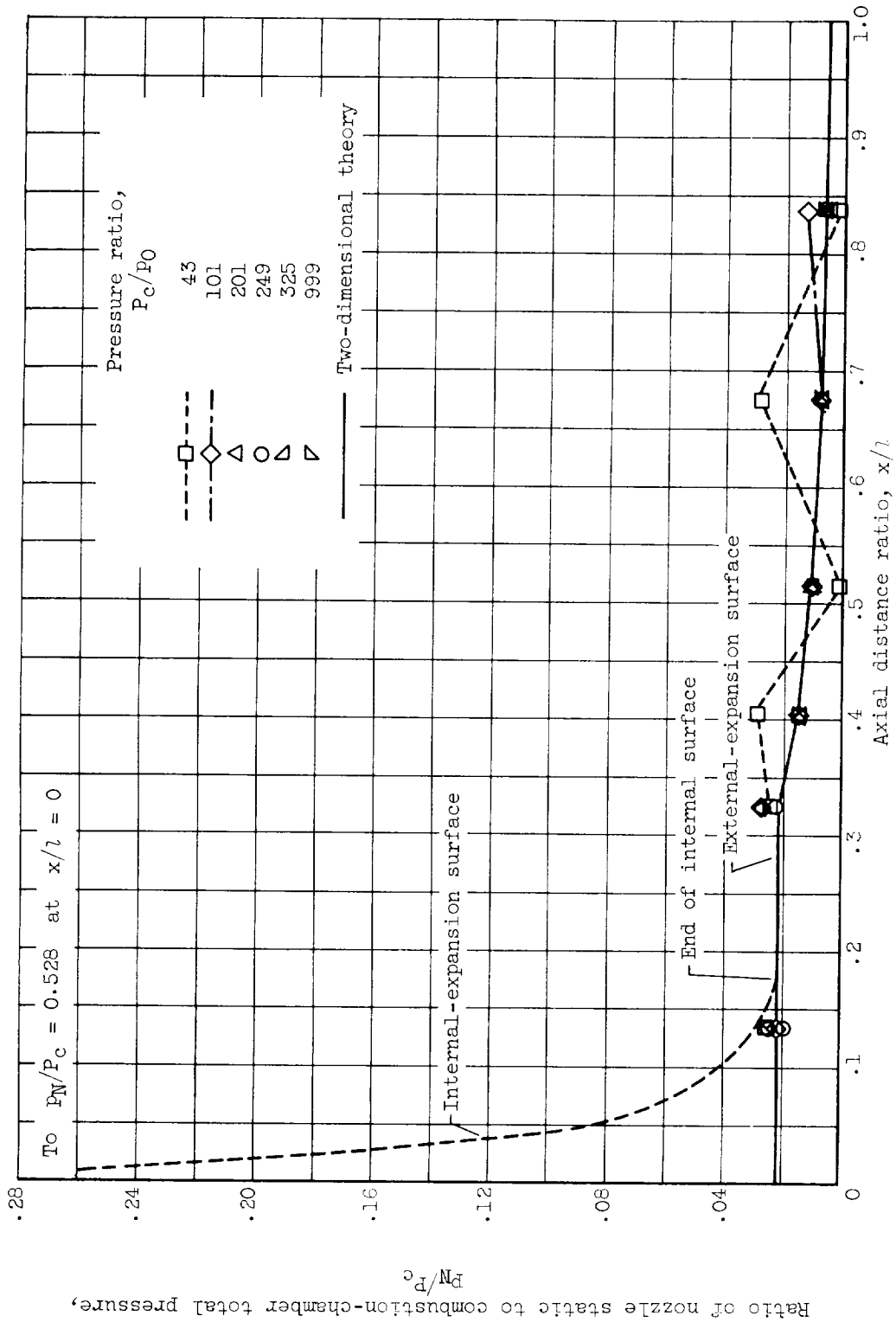

(a) Area ratio, ϵ, 15; nozzle length, l, 9.25 inches.

Figure 9. - Annular-nozzle pressure distributions.

E-1719

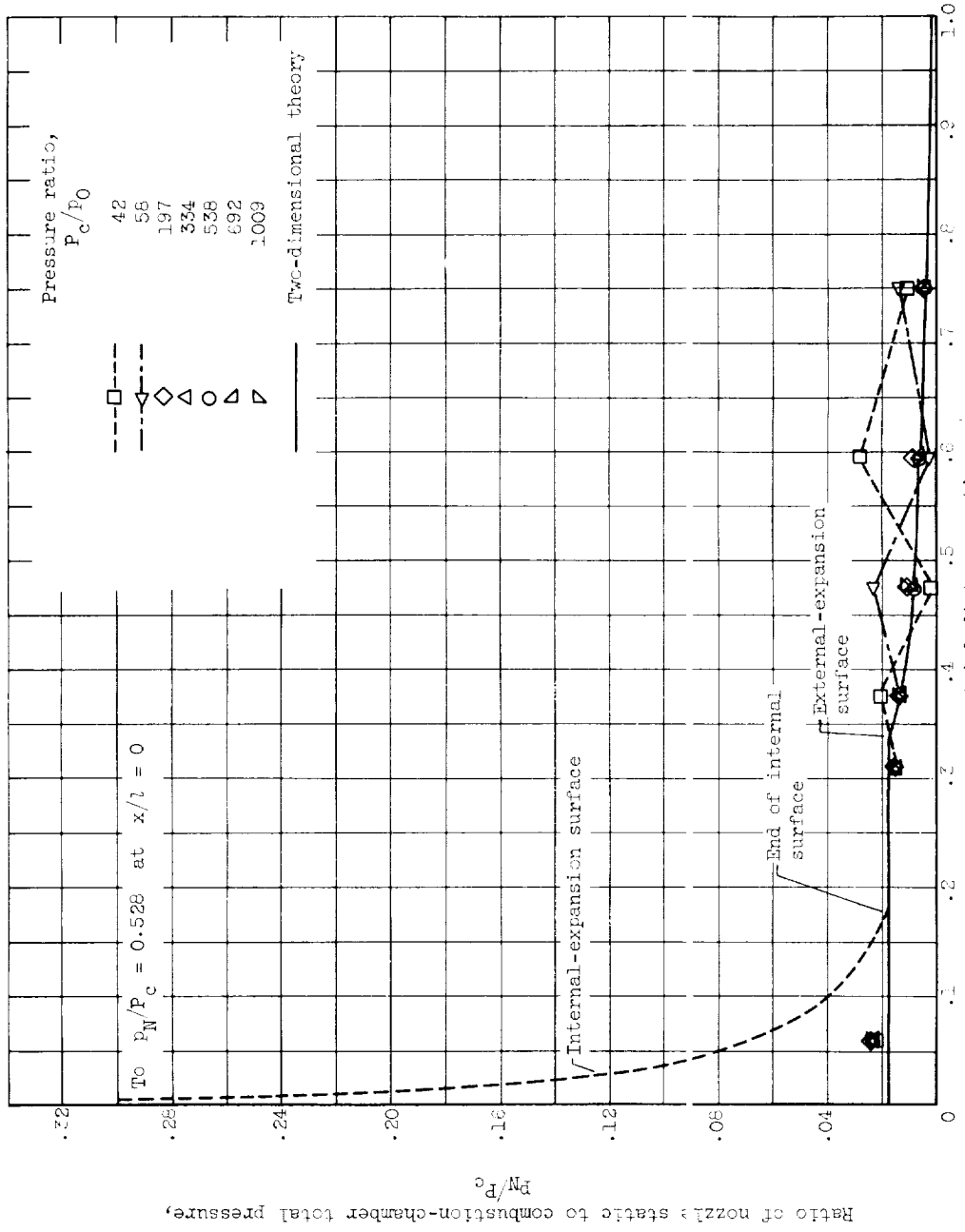

(b) Area ratio, ϵ, 25; nozzle length, l, 7.97 inches.

Figure 3. - Concluded. Annular-nozzle pressure distributions.

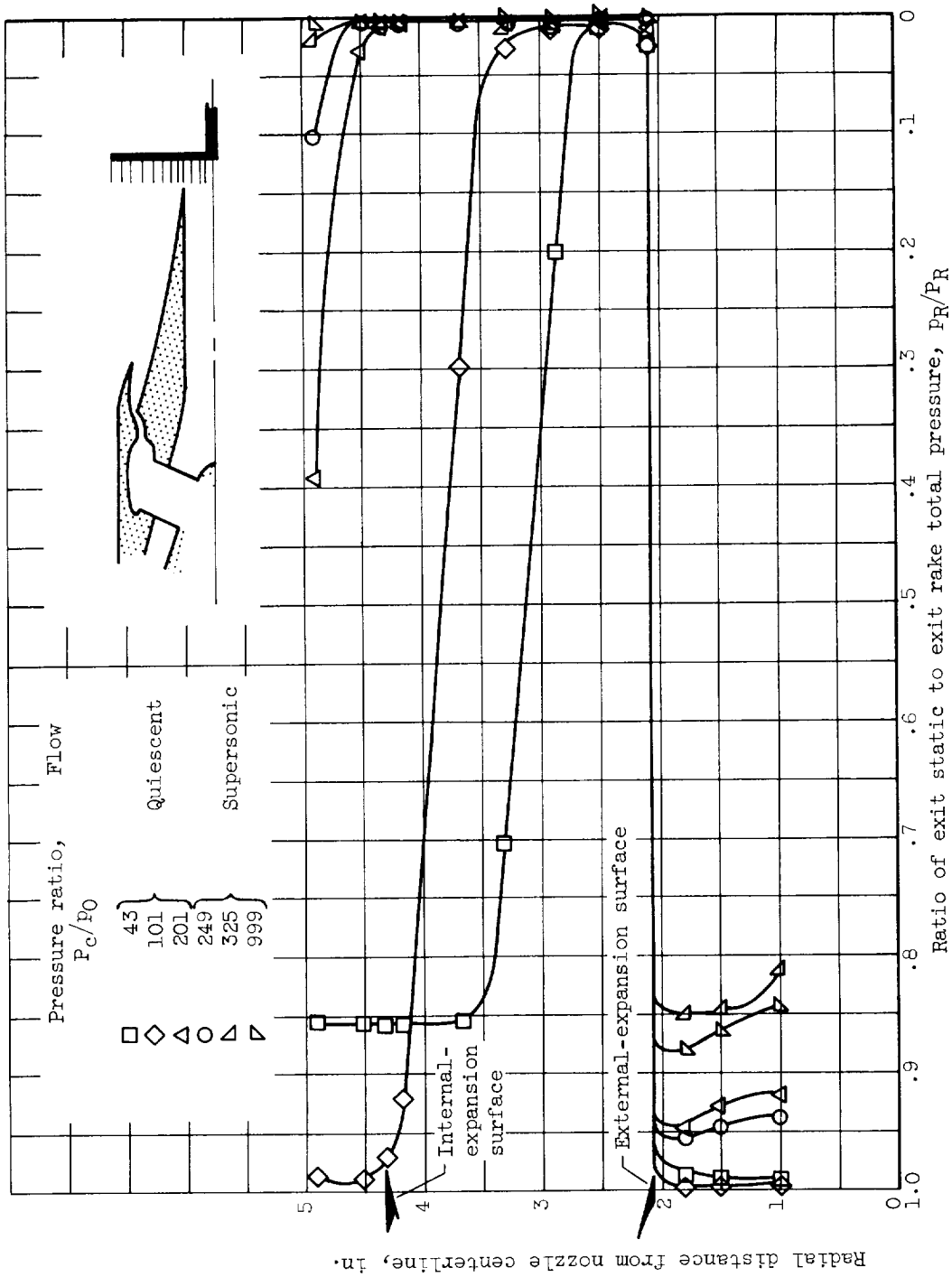

(a) Area ratio, ϵ, 15.

Figure 10. - Exit pressure profiles for annular nozzles.

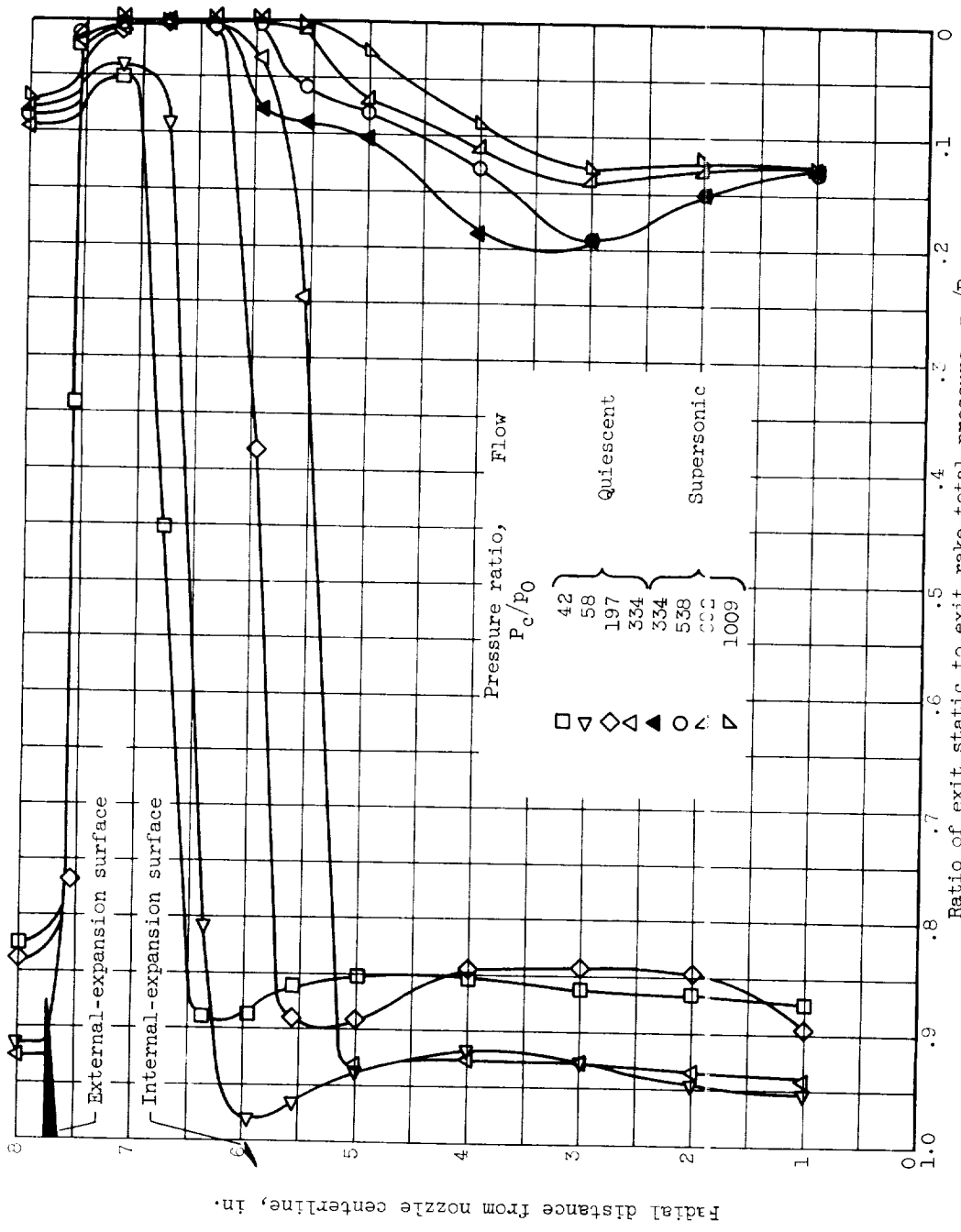

(b) Area ratio, ϵ, 25.

Figure 10. - Concluded. Exit pressure profiles for annular nozzles.

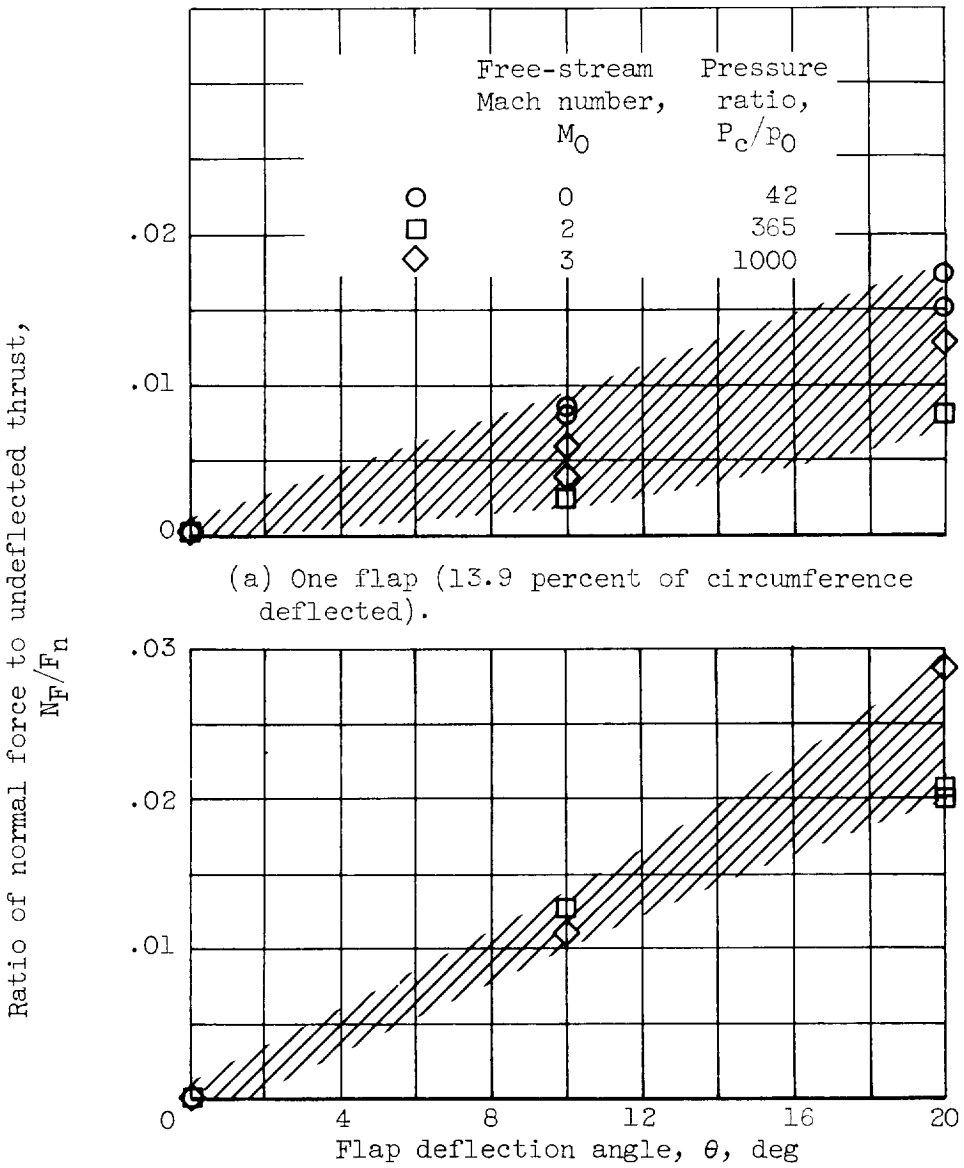

(a) One flap (13.9 percent of circumference deflected).

(b) Both flaps (27.8 percent of circumference deflected).

Figure 11. - Effectiveness of nozzle flaps for guidance control on area-ratio-15 annular nozzle.

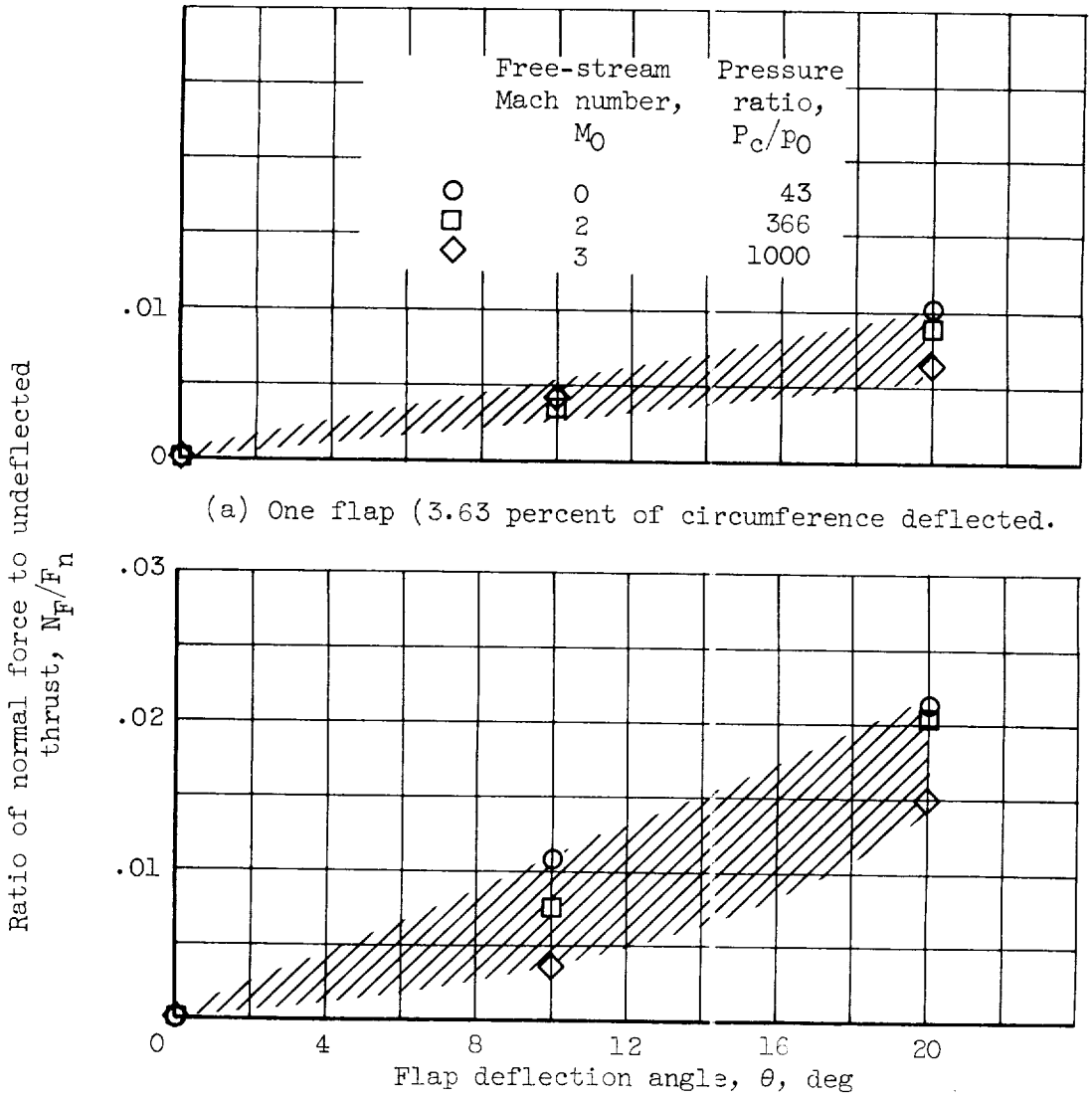

(a) One flap (3.63 percent of circumference deflected.

(b) Both flaps (7.26 percent of circumference deflected).

Figure 12. - Effectiveness of nozzle flaps for guidance control on area-ratio-25 nozzle.

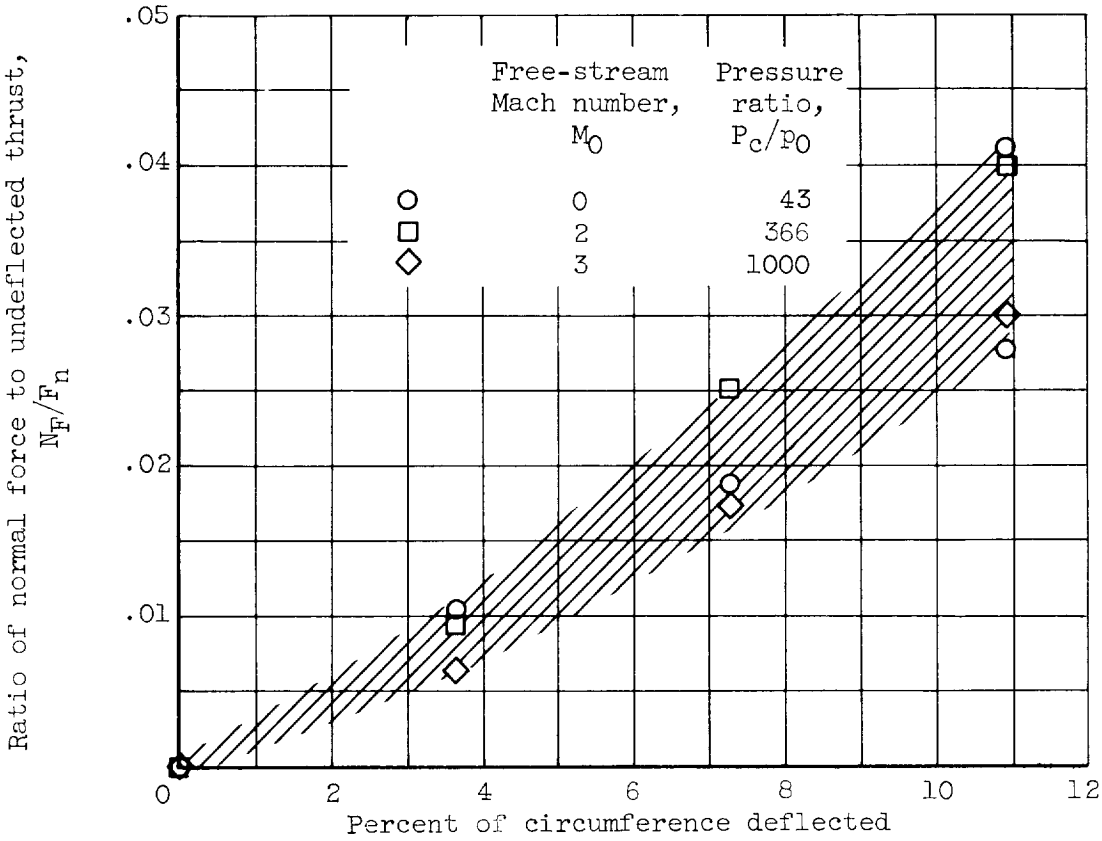

Figure 13. - Effect of flap width on flap effectiveness for area-ratio-25 nozzle. Single flap.

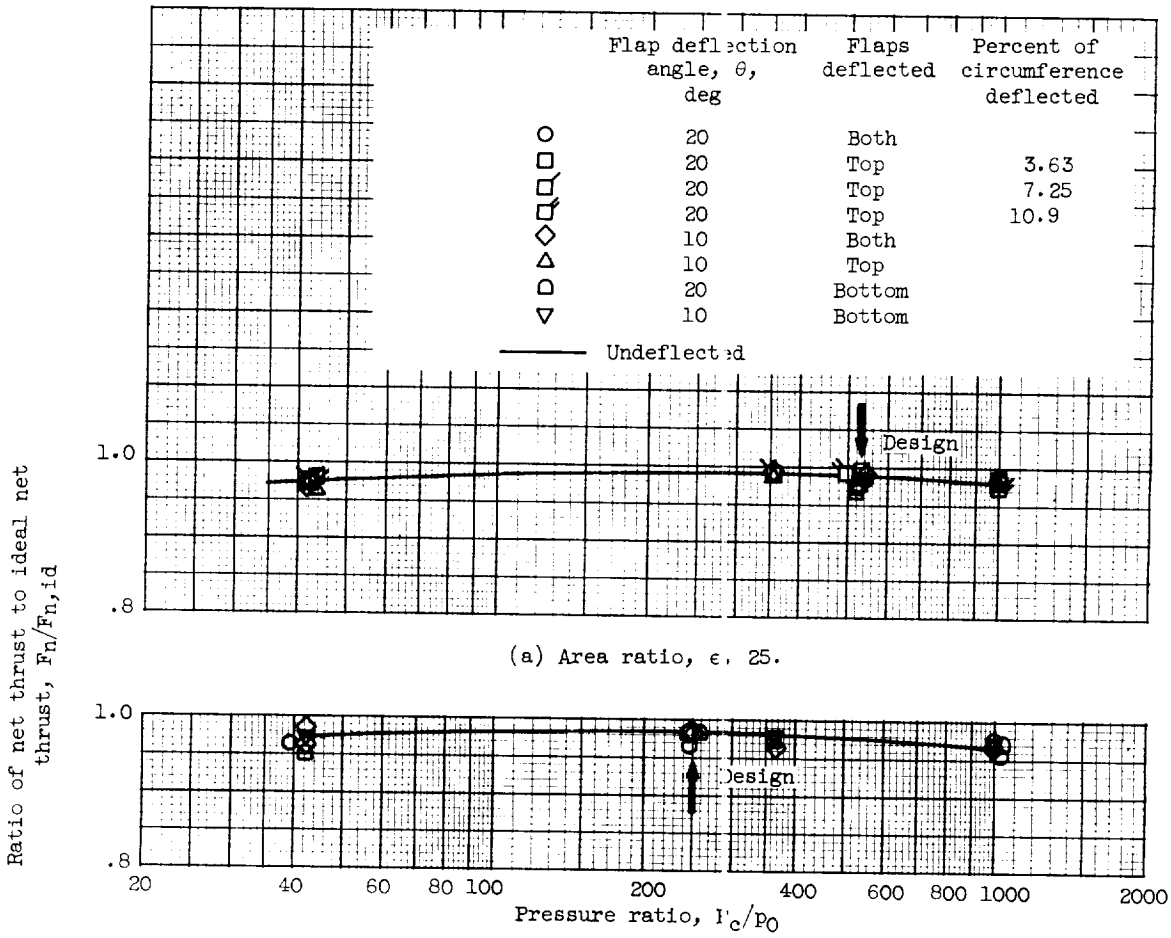

(a) Area ratio, ϵ, 25.

(b) Area ratio, ϵ, 15.

Figure 14. - Annular-nozzle thrust performance at Mach 0, 2, and 3 with nozzle flaps installed.

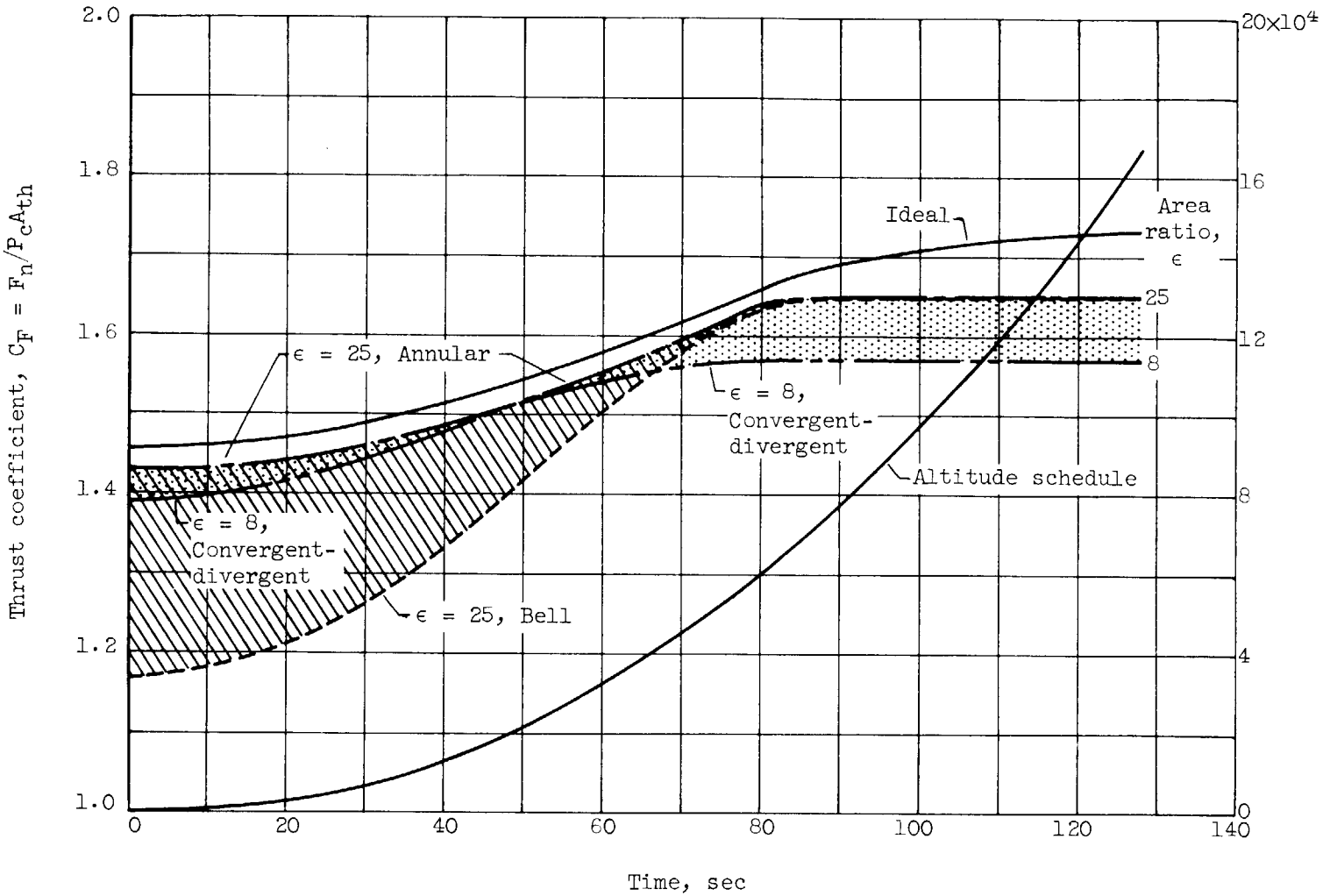

Figure 15. - Thrust-coefficient comparison for typical boost trajectory with burnout at 167,200 feet. Combustion-chamber pressure, P_c, 600 pounds per square inch absolute.